ACS OMEGA

http://pubs.acs.org/journal/acsodf

Article

High Power Density Direct Formate Microfluidic Fuel Cells with the Different Catalyst-Free Oxidants

Chunmei Liu,* Yanjun Gao, Lei Liu, Canxing Sun, Pengfei Jiang, and Jingjie Liu

Cite This: *ACS Omega* 2022, 7, 28646−28657

Read Online

ACCESS | Metrics & More | Article Recommendations | Supporting Information

ABSTRACT: As micropower devices, microfluidic fuel cells (MFCs) have gained much attention due to their simple configurations and high power densities. MFCs exploit the parallel laminar flowing of two electrolytes in a microchannel with a characteristic length from 1 to 1000 μm to separate the anolyte and catholyte, without the proton exchange membranes in the traditional fuel cells. These membrane-less configurations can avoid a series of technical problems related to the membranes. To achieve an MFC with high power density and low cost, we constructed the direct formate MFCs with two catalyst-free oxidants containing $FeCl_3$ and $Na_2S_2O_8$ solutions, respectively, and compared the performance of the two MFCs. Due to $Na_2S_2O_8$ being an oxidant with some distinctive advantages, including its high theoretical potential, high solubility of itself and its reduction product, and environmental friendliness, the $Na_2S_2O_8$-based MFC showed a higher open-circuit voltage (>2.0 V) and better performance. Then, we studied the effects of oxidant concentrations, flow rates, and fuel concentrations on the performance of the $Na_2S_2O_8$-based MFC. The results showed the optimum performance of the $Na_2S_2O_8$-based MFC with the peak power density of 214.95 mW cm^{-2} and the limiting current density of 700.13 mA cm^{-2} under the conditions of 1.5 M HCOONa, 2 M $Na_2S_2O_8$, and 300 μL min^{-1} at an anolyte/catholyte flow ratio of 2:1. The performance was also the highest among the direct formate MFCs reported up to now. Moreover, the $Na_2S_2O_8$-based MFC could stably discharge for about 4 h under a constant voltage. All of the results demonstrated that $Na_2S_2O_8$ was a suitable oxidant and that the $Na_2S_2O_8$-based MFC could realize the goals of high power density and low cost for the actual application of MFCs.

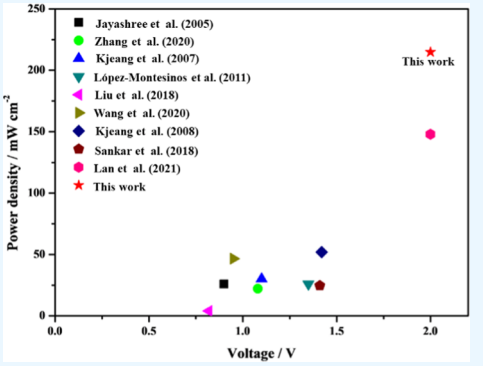

1. INTRODUCTION

Microfluidic fuel cells (MFCs), as micropower portable electronics, have attracted enormous attention from researchers since it was first presented and demonstrated in 2002.[1] MFCs exploit the parallel laminar flowing of aqueous electrolytes in a microchannel to naturally separate the anolyte and catholyte, removing the proton exchange membranes generally used in the traditional fuel cells.[2,3] The membrane-less MFC configurations not only simplify the construction of the MFCs and lower the cell cost, but also eliminate the problems relevant to the membranes, such as membrane degradation and electrolyte crossover.[4,5] As micropower devices, MFCs have potential applications in fields such as medical diagnostics, wearable healthcare devices, and smart logistics.[6]

To date, different fuels have been used in MFCs, mainly including hydrogen,[7,8] methanol,[9,10] formic acid,[11,12] formate,[13,14] vanadium redox species,[15,16] and hydrogen peroxide.[17,18] Most hydrocarbon fuels could produce carbon dioxide (CO_2) during the electrochemical conversion processes. Usually, CO_2 develops as a gaseous product in an acid or neutral electrolyte, especially under high current densities.[12] Formic acid has been established as a fuel with high energy density[19,20] and its oxidation kinetics on the Pd catalysts are rapid, thereby achieving higher power densities than methanol fuels.[21] Compared with the acid and neutral electrolytes, alkaline electrolytes could absorb a large amount of CO_2 as carbonates and also benefit carbon sequestration. Formate displays faster oxidation kinetics in alkaline electrolytes than in acidic electrolytes.[22,23] In addition, formate has nonflammable and nontoxic advantages, benefiting its promising applications. The formate oxidation in alkaline media is shown via the following equation.

$$HCOO^- + 3OH^- \rightarrow CO_3^{2-} + 2H_2O + 2e^- \quad E^0 = -1.05 \text{ V vs SHE} \tag{1}$$

Until now, the oxidants often adopted in MFCs are oxygen,[11,24] hypochlorite,[25] hydrogen peroxide,[12] potassium

Received: June 20, 2022
Accepted: July 25, 2022
Published: August 2, 2022

Table 1. Theoretical Potentials of the Oxidants Used in the MFCs

oxidant	reduction reaction	theoretical potential (V vs SHE)	catalyst	reference
O_2	$O_2 + 4H^+ + 4e^- \rightarrow 2H_2O$	+1.23	Pt	24
ClO_4^-	$ClO_4^- + H^+ + 2e^- \rightarrow Cl^- + H_2O$	+1.48	Au	25
H_2O_2	$H_2O_2 + 2H^+ + 2e^- \rightarrow 2H_2O$	+1.78	Pt	12
$Cr_2O_7^{2-}$	$Cr_2O_7^{2-} + 14H^+ + 6e^- \rightarrow 2Cr^{3+} + 7H_2O$	+1.33	MoO_3	32
		+1.78	none	31
$KMnO_4$	$MnO_4^- + 4H^+ + 3e^- \rightarrow MnO_2 + 2H_2O$			
VO_2^+	$VO_2^+ + 2H^+ + e^- \rightarrow VO^{2+} + H_2O$	+0.10	none	27
Br_2	$Br_2 + 2e^- \rightarrow 2Br^-$	+1.10	none	33
Fe^{3+}	$Fe^{3+} + e^- \rightarrow Fe^{2+}$	+0.77	none	28 29,
$S_2O_8^{2-}$	$S_2O_8^{2-} + 2e^- \rightarrow 2SO_4^{2-}$	+2.01	none	14

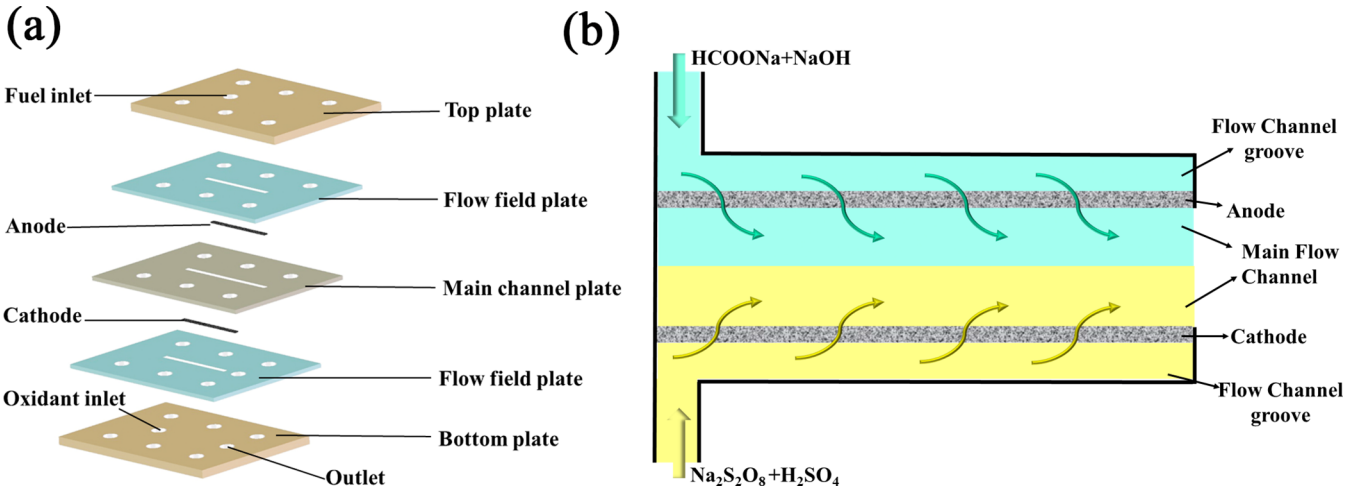

Figure 1. Schematic diagram of the construction of the MFC (a) and flowing state of the fuel and oxidant solutions inside the MFC (b).

permanganate,[26] vanadium oxide,[15,27] ferric iron ions,[28,29] and persulfate.[14] The theoretical potentials of these oxidants are displayed in Table 1. The performance of the MFC with dissolved oxygen as the oxidant was limited by the low solubility of oxygen in the solutions.[30] To improve the mass transfer of dissolved oxygen and increase the oxygen reduction reaction rate, gaseous oxygen from the air was directly used as the oxidant of MFCs, called as the air-breathing cathode.[11]

However, the adoption of oxygen as the oxidant often needs Pt or Pt-based noble metals as the catalysts, which can vastly increase the MFC cost. Some liquid oxidants such as hypochlorite and hydrogen peroxide also require Au, Pt, or Pd noble metals as the catalysts to fasten their reduction reactions and achieve better performance. Under these noble catalysts, the H_2O_2 reduction reaction takes place and simultaneously, the oxygen gas evolves due to the H_2O_2 decomposition, disturbing the laminar flow state of the fluids and inducing the reactant crossover. Other liquid oxidants such as $KMnO_4$ and VO_2^+ can undergo the reduction reactions without any catalysts. However, the insoluble products of MnO_2 from the reduction reaction of $KMnO_4$ can adhere to the electrode surface and block the contact between the oxidant solution and the electrode, decreasing the cell performance.[26,31] Vanadium ions not only pollute soil and water resources but also impair the health of people and animals, owing to their toxicity.[14] Ferric ions as the oxidants own many advantages such as fast reduction kinetics, large water solubility, no gas production during reduction, inexpensiveness, and environmental benignity. In our previous research,[28] we have investigated the four different ferric salts as oxidants in the MFCs and concluded that the performance of the MFC with ferric chloride ($FeCl_3$) as the oxidant was the best. However, the open-circuit voltage of the MFC with the ferric ions as the oxidant was not high (<1.0 V) due to the low electrode potential (+0.77 V vs SHE) of the ferric ions.

Persulfate has been widely adopted to treat wastes and pollutants as it can produce the highly active free radicals during the advanced oxidation processes.[34,35] Moreover, persulfate has been used as an electron acceptor in microbial fuel cells[36] and photocatalytic fuel cells.[37] The prominent advantage of persulfate is its high electrode potential (+2.01 V vs SHE). Yet, in the microfluidic fuel cells, persulfate as the cathodic oxidant of the MFC has seldom been reported to date.

To achieve an MFC with a high power density and low cost, while at the same time choosing oxidants with strong reducing features and environmental friendliness, we constructed the direct formate microfluidic fuel cells with the two catalyst-free oxidants $FeCl_3$ and $Na_2S_2O_8$, and then compared the performance of the two MFCs. Given the higher theoretical potential and stronger reduction of persulfate between the two oxidants, the open-circuit voltage (OCV) and the performance of the $Na_2S_2O_8$-based MFC was higher and better. The effects of the operational parameters, including the oxidant concentrations, flow rates of the two solutions, and fuel concentrations, on the $Na_2S_2O_8$-based MFC were investigated. In addition, the discharge performance of the $Na_2S_2O_8$-based MFC was tested to evaluate the cell stability.

https://doi.org/10.1021/acsomega.2c03840
ACS Omega 2022, 7, 28646−28657

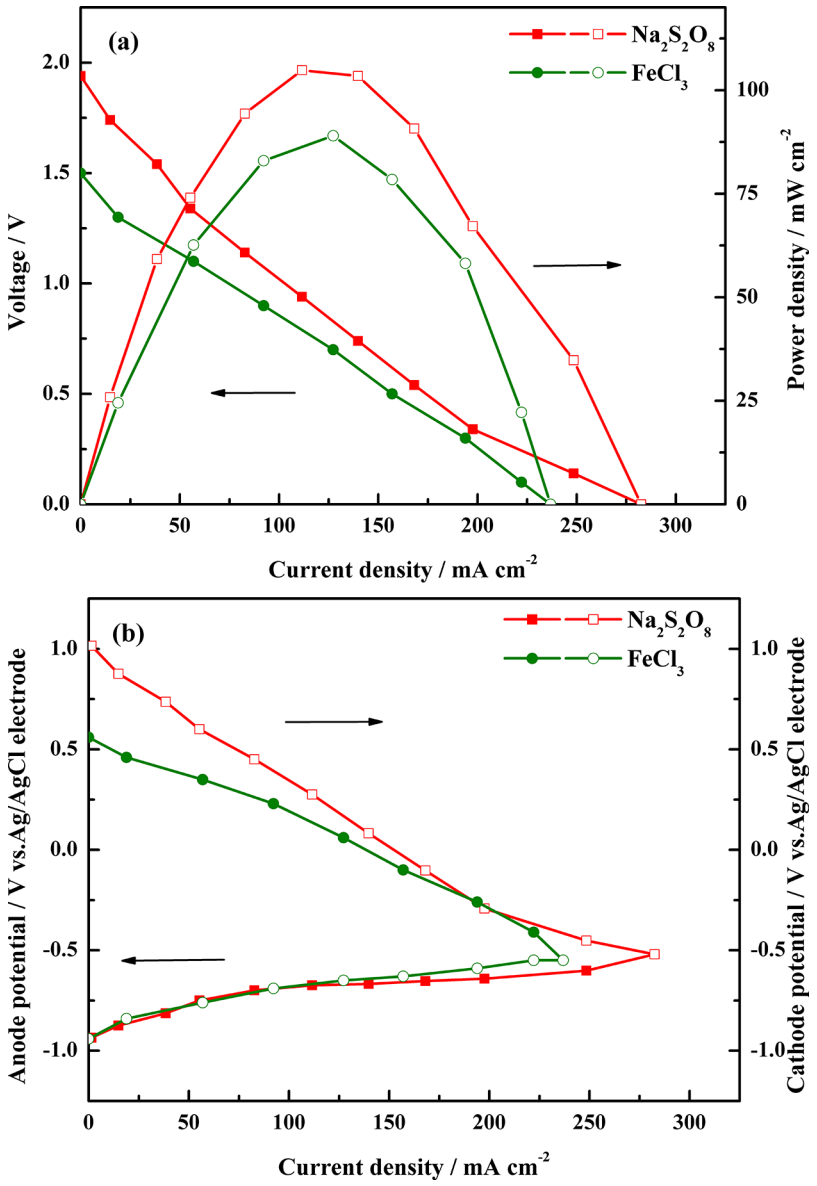

Figure 2. Polarization curves (a) and electrode potentials curves (b) of the MFCs with the two catalyst-free oxidants.

2. EXPERIMENTAL SECTION

In the experiment, carbon paper (HCP020N, Shanghai Hesen Co., Ltd., China) electrodes with dimensions of 2.0 mm (width) × 15 mm (length) × 0.2 mm (height) were adopted as the anode and cathode, respectively. Before use, the electrodes were treated in the muffle furnace at 450 °C for 10 h to improve their hydrophilicities. After heat treatment, the carbon paper without any catalyst loading was directly used as the cathode. As the anode electrode, the Pd catalyst was electrochemically deposited on the carbon paper at a potential of 0.0 V vs Ag/AgCl using an electrochemical workstation (Zennium Zahner, Germany) in a three-electrode mode until the Pd loading was 5 mg cm^{-2}. The electroplating solution consisted of 1.0 wt % $PdCl_2$ in 1 M HCl solution.[14,25] The surface morphologies of the anode with the Pd catalyst and the crystal size of the Pd catalyst could be found in our previous work.[28,29] In brief, the Pd catalyst presented a dendritic structure with the different sizes of the branches, as observed from the scanning electron microscopy (SEM) image of the Pd catalyst on the carbon paper electrode. The average size of the Pd catalyst was 10.6 nm according to the Pd (220) facet using the Debye−Scherrer equation.

The structure of the MFC is schematically shown in Figure 1a. The MFC was made of five poly(methyl methacrylate) (PMMA) plates: two cover plates, two flow field plates with groove dimensions of 15 mm (length) × 1 mm (width) × 1 mm (height), and one main flow channel plate with flow channel dimensions of 15 mm (length) × 1 mm (width) × 1 mm (height). There existed one 3 mm hole in the upper cover plate as the fuel inlet and two 3 mm holes in the bottom cover plate as the oxidant inlet and outlet, respectively. To make the solutions flow uniformly through the carbon paper, the groove size of the flow field plate was kept smaller than that of the electrode. The active electrode surface area was its vertical projected area of 0.15 cm^2 (15 mm × 1 mm).

The anolyte consisted of sodium formate as the fuel and sodium hydroxide as the anodic supporting electrolyte. The catholytes were made of the two aqueous oxidants and their corresponding supporting electrolytes. The supporting electrolytes were used to improve the solution conductivities and

https://doi.org/10.1021/acsomega.2c03840
ACS Omega 2022, 7, 28646−28657

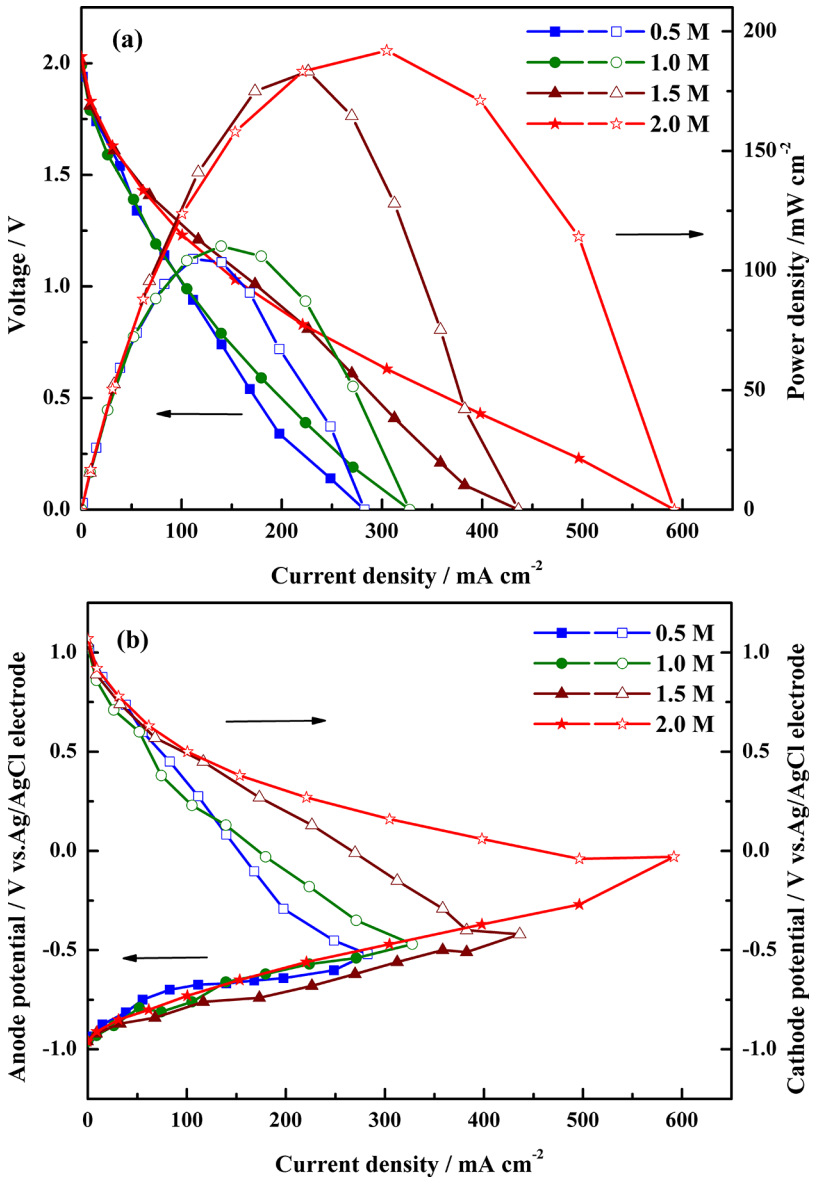

Figure 3. Polarization curves (a) and electrode potentials curves (b) of the $Na_2S_2O_8$-based MFC under the different $Na_2S_2O_8$ concentrations.

decrease the cell resistances. The anolyte and catholyte were injected into the MFC by a syringe pump (LSP02-1B, Baoding Longer Precision Pump Co., Ltd., China). The fuel and oxidant solutions were injected into the inlets and grooves of the flow field plates, then transported through the porous electrodes into the main flow channel and out of the outlet. The schematic diagram of the two solutions flowing inside the MFC is shown in Figure 1b.

The cell performance was measured using the electrochemical workstation with the chronoamperometry method from the open-circuit voltage to 0.0 V with −200 mV intervals per step within 60 s. The currents were gained and recorded at the end of each voltage step. The discharge performance of MFC was obtained under the constant cell voltage in a two-electrode mode with the cathode electrode as the working electrode and the anode electrode as the reference and counter electrode.

The cathode potentials were achieved using the data acquisition unit (Agilent 34972 A) through the potential difference between the cathode electrode and the Ag/AgCl reference electrode. The Ag/AgCl reference electrode in the saturated KCl solution was put in the MFC outlet. The anode potentials were obtained by subtracting the cell voltages from the cathode potentials. The current densities and power densities were all calculated on the basis of the active electrode surface area (0.15 cm^2). The reduction performance of the persulfate was tested using the linear sweep voltammetry (LSV) method at a scan rate of 10 mV s^{-1} from −0.5 to +1.1 V. Also, the oxidation of sodium formate was measured by cyclic voltammetry (CV) at a scan rate of 10 mV s^{-1} with the potential range from −1.0 to 0.4 V. The LSV and CV experiments were carried out in a three-electrode mode, wherein the carbon paper was used as the working electrode, the Pt sheet (10 mm × 50 mm) as the counter electrode, and the Ag/AgCl electrode in the saturated KCl solution as the reference electrode.

All of the tests were measured at least three times to obtain reliable experimental results at temperatures of 293 ± 2 K.

https://doi.org/10.1021/acsomega.2c03840
ACS Omega 2022, 7, 28646−28657

3. RESULTS AND DISCUSSION

3.1. Effect of Different Cathode Oxidants. We compared the performance of the direct formate microfluidic fuel cells with the two different oxidants when the anodic and cathodic flow rates were 200 and 100 μL min^{-1}, respectively. The anolyte comprised a 0.5 M HCOONa + 2 M NaOH solution. The two catholytes were a 0.5 M $Na_2S_2O_8$ + 1 M H_2SO_4 solution and a 0.5 M $FeCl_3$ + 1 M H_2SO_4 solution, respectively. In the anolytes and catholytes, NaOH and H_2SO_4 solutions were used as the supporting solutions to provide high-concentration ions and decrease the solution resistances. The performance of the direct formate MFCs with the two oxidants is shown in Figure 2.

From Figure 2, it could be seen that the open-circuit voltage (OCV) of the $Na_2S_2O_8$-based MFC was ~2.0 V, far larger than the OCV (~1.5 V) of the $FeCl_3$-based MFC. These differences could be ascribed to the disparities in the electrode potentials, especially in the cathode potentials. As seen from Figure 2b, the cathode potentials of the $Na_2S_2O_8$-based MFC were higher due to the larger theoretical potential and stronger reducibility of $Na_2S_2O_8$ among the MFC oxidants. Thus, the voltages of the $Na_2S_2O_8$-based MFC always were higher between the two MFCs. The peak power density and limiting current density of the $Na_2S_2O_8$-based MFC was 104.87 mW cm^{-2} and 282.53 mA cm^{-2}, respectively, while those of the $FeCl_3$-based MFC were 89 mW cm^{-2} and 236.87 mA cm^{-2}. The peak power density of the $Na_2S_2O_8$-based MFC was 1.17 times that of the $FeCl_3$-based MFC.

The OCV (~2.0 V) of the $Na_2S_2O_8$-based MFC was far lower than its theoretical cell voltage (3.06 V) as its cathode potential (~1.21 V vs SHE) under the open circuit was much less than the theoretical cathode potential (2.0 V vs SHE). This phenomenon could be ascribed to two reasons: (1) the persulfate showed a high activation loss due to its low reaction rate under room temperature,[38] and (2) the persulfate could slowly react with water to produce oxygen[39] and the reduction reaction of oxygen could decrease the cathode potentials.

Now we have testified that the performance of the direct formate MFC with $Na_2S_2O_8$ as the oxidant was better. In the subsequent experiments, we investigated the effects of the oxidant concentrations, flow rates, and fuel concentrations on the performance of the $Na_2S_2O_8$-based MFC.

3.2. Effect of $Na_2S_2O_8$ Concentrations on the Performance of the $Na_2S_2O_8$-Based MFC. $Na_2S_2O_8$ as the oxidant plays a crucial role in the MFC performance. The effect of $Na_2S_2O_8$ concentrations from 0.5 to 2.0 M (lower than its maximum soluble concentration of 2.3 M) on the MFC performance was investigated and the results are shown in Figure 3. During this experiment, the anodic and cathodic flow rate was 200 and 100 μL min^{-1}, respectively. The anolyte comprised a 2 M NaOH and 0.5 M HCOONa solution, while the H_2SO_4 concentration in the catholyte remained at 1 M.

As seen from Figure 3a, the peak power density and limiting current density of the $Na_2S_2O_8$-based MFC increased with the increase of the oxidant concentrations. At 2 M $Na_2S_2O_8$, the MFC performance reached the best with the peak power density of 191.94 mW cm^{-2} and limiting current density of 591.8 mA cm^{-2}. The maximum power density at 2 M $Na_2S_2O_8$ was about 2.09 times as high as that at 0.5 M $Na_2S_2O_8$. The peak power densities and limiting current densities of the MFCs with the different $Na_2S_2O_8$ concentrations are shown in Table 2.

Table 2. Peak Power Densities and Limiting Current Densities of the MFCs under the Different $Na_2S_2O_8$ Concentrations

$Na_2S_2O_8$ concentration	peak power density (mW cm^{-2})	limiting current density (mA cm^{-2})
0.5 M	104.84	282.53
1.0 M	110.18	327.6
1.5 M	183.28	436.07
2.0 M	191.94	591.8

The enhancement in the cell performance was mainly caused by the increase of the cathode potentials (shown in Figure 3b). Higher cathode oxidant concentrations could lead to stronger reducibility, more positive cathode potentials, and better cathode performance. This was verified by the LSV curves (Figure 4) for the different $Na_2S_2O_8$ oxidant concentrations.

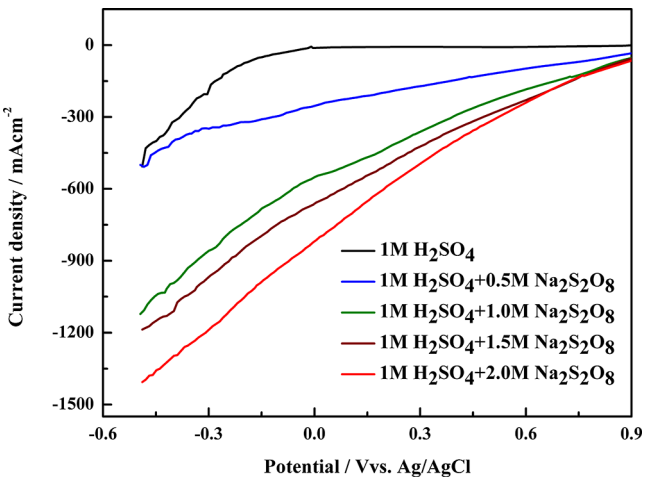

Figure 4. LSV curves under the different $Na_2S_2O_8$ concentrations.

As shown in Figure 4, the onset potentials (~1.0 V vs Ag/AgCl) of the persulfate reduction reaction were almost the same, while the current densities under the different $Na_2S_2O_8$ concentrations were obviously different, especially at the lower potentials. With the increase in the $Na_2S_2O_8$ concentrations, the current densities in the LSV curves became larger. At 2 M $Na_2S_2O_8$, the largest current density of 1122.43 mA cm^{-2} was achieved, which implied that 2 M $Na_2S_2O_8$ could lead to the strongest reduction.

3.3. Effect of Flow Rates on the Performance of the $Na_2S_2O_8$-Based MFC. Flow rates are crucial to keep a steady and laminar flow in a microchannel. To validate the effects of the flow rates on the performance of the $Na_2S_2O_8$-based MFC, we changed the total flow rates and the anolyte/catholyte flow ratios, respectively. The catholyte was a 2.0 M $Na_2S_2O_8$ + 1.0 M H_2SO_4 solution and the anolyte was a 0.5 M HCOONa + 2.0 M NaOH solution.

Firstly, the total flow rates increased from 150 to 450 μL min^{-1}, while the anolyte/catholyte flow rate ratio was kept at 2:1. The effects of the total flow rates on the performance of the $Na_2S_2O_8$-based MFCs are shown in Figure 5.

From Figure 5a, it can be seen that as the total flow rate increased from 150 to 300 μL min^{-1}, the performance of the $Na_2S_2O_8$-based MFC was obviously improved. However, the total flow rate was further increased to 450 μL min^{-1}, and the power output of the $Na_2S_2O_8$-based MFC decreased. At 300

https://doi.org/10.1021/acsomega.2c03840
ACS Omega 2022, 7, 28646−28657

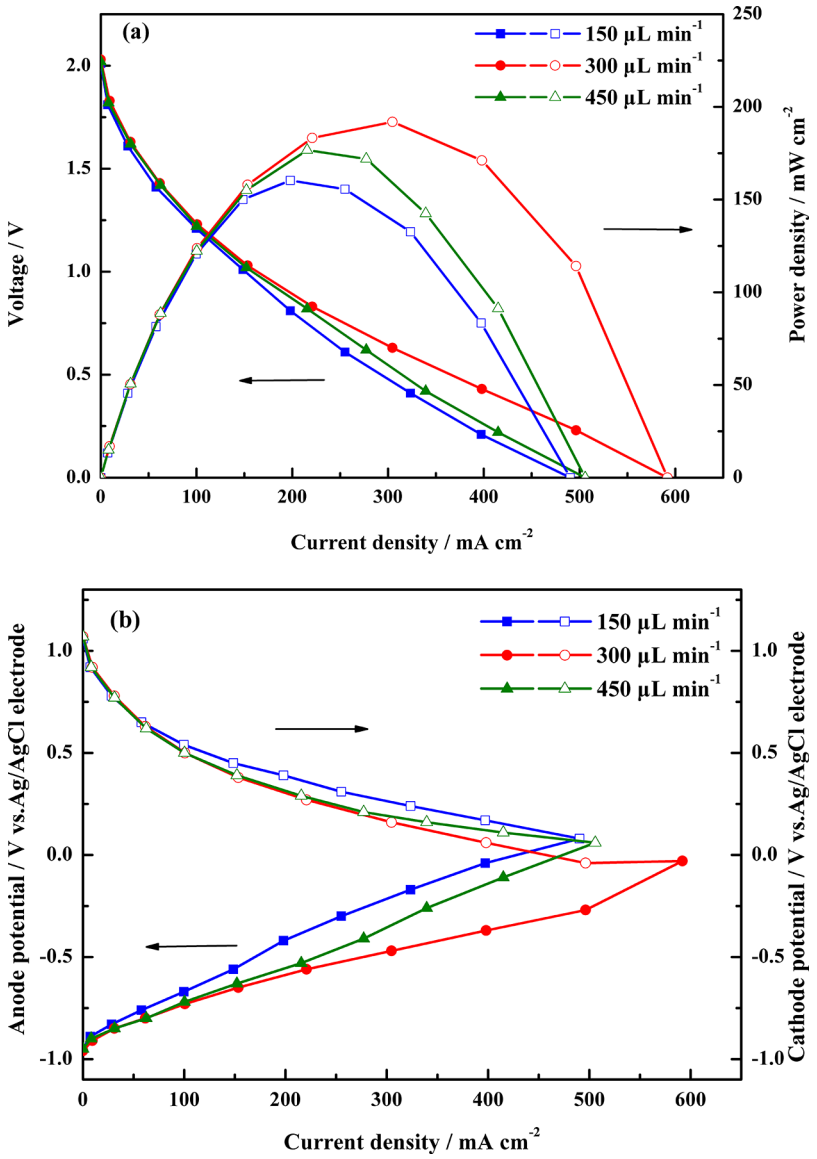

Figure 5. Polarization curves (a) and electrode potentials curves (b) of the $Na_2S_2O_8$-based MFC with the different total flow rates.

μL min^{-1}, the performance of the $Na_2S_2O_8$-based MFC was the optimum, with the peak power density of 191.94 mW cm^{-2} and limiting current density of 591.8 mA cm^{-2}. The largest power density of the MFC at 300 μL min^{-1} was 1.2 times that at 150 μL min^{-1}. The peak power densities and limiting current densities of the MFCs with the different total flow rates are listed in Table 3.

To explain the trends of the performance of the MFC with the total flow rates, we collected the electrode potential curves at the different total flow rates. As seen from Figure 5b, the discrepancy of anode potentials at the different flow rates was larger than that of cathode potentials. This implied the flow rates had a more prominent effect on the anode performance than on the cathode performance. When the total flow rate increased to 300 μL min^{-1}, the anode electrode potentials became more negative and the anode performance was improved, as the higher flow rate could bring more anolyte to the electrode and benefit the fuel transport to the electrode. When more anolyte was delivered into the micro main channel, more OH^- ions from the anolyte could diffuse to the catholyte and increase the pH of the catholyte. It has been testified that the electrochemical reaction rate of $Na_2S_2O_8$ improved with the increase of the H^+ ion concentration in acidic solution.[14] Enhancement in pH of the catholyte decreased the cathode electrode potential with the increase of the total flow rate (Figure 5b). On further increasing the total flow rate to 450 μL min^{-1}, as seen from Figure 5b, the anode potentials at the middle and high current densities (>215.53 mA cm^{-2}) became more positive. Especially at the cell voltage of 0.0 V, the anodic potential obtained was +0.06 V (vs Ag/AgCl). The flow rate (450 μL min^{-1}) was too high and the reactant solutions flew out of the cell before they could be

Table 3. Peak Power Densities and Limiting Current Densities of the MFCs with the Different Total Flow Rates

total flow rate	peak power density (mW cm^{-2})	limiting current density (mA cm^{-2})
150 μL min^{-1}	160.38	490.33
300 μL min^{-1}	191.94	591.8
450 μL min^{-1}	176.74	505.87

https://doi.org/10.1021/acsomega.2c03840
ACS Omega 2022, 7, 28646−28657

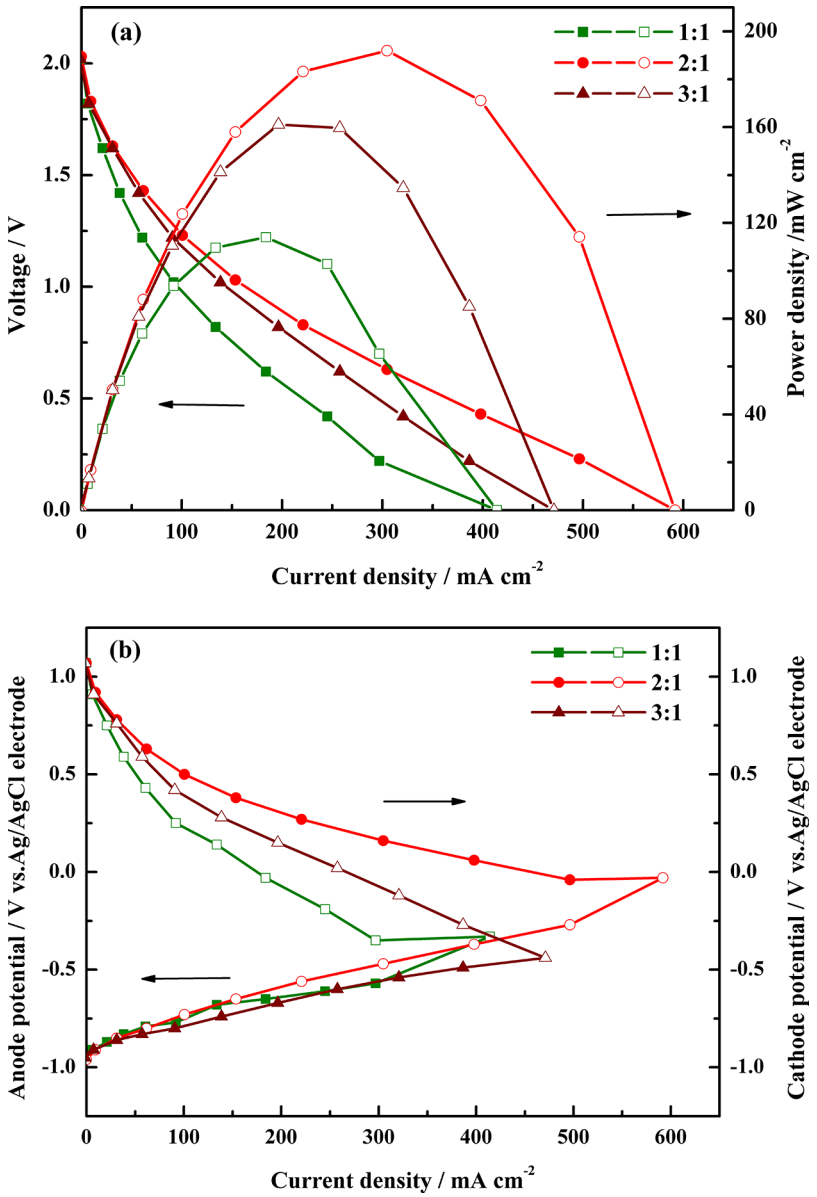

Figure 6. Polarization curves (a) and electrode potential curves (b) of the $Na_2S_2O_8$-based MFC with the different anolyte/catholyte flow ratios at the total flow rate of 300 μL min^{-1}.

thoroughly reacted, so the anodic potentials increased and the cathode potentials decreased.

Then, at the total flow rate of 300 μL min^{-1}, we studied the effect of the different anolyte/catholyte flow rate ratios, 150:150 μL min^{-1} (1:1), 200:100 μL min^{-1} (2:1), and 225:75 μL min^{-1} (3:1), on the cell performance, as shown in Figure 6.

As shown in Figure 6, as the anolyte/catholyte flow ratio increased from 1:1 to 2:1, the cell performance was improved. When the flow ratio was further increased to 3:1, the cell performance began to descend. At the anolyte/catholyte flow ratio of 2:1, the cell performance was the best. The maximum power density at the flow rate of 2:1 was 1.05 times that at 1:1 and 1.17 times that at 3:1, respectively. The peak power densities and limiting current densities of the MFC under the different anolyte/catholyte flow ratios are listed in Table 4.

From Figure 6b, it was evident that, under the different flow ratios, the MFC performance difference was mainly limited by the cathode performance. When the flow ratio increased from 1:1 to 2:1, the catholyte flow rate decreased from 150 to 100 μL min^{-1}, while the cathode potentials were improved. This could be ascribed to the more sufficient contact between the oxidant solution and the cathode electrode under the lower flow rate, enhancing the cathode reaction and improving the cathode potentials. When the flow ratio further increased from 2:1 to 3:1 and the catholyte flow rate declined to 75 μL min^{-1}, the cathode potentials were decreased. This could be attributed to the less oxidant transport to the cathode due to

Table 4. Peak Power Densities and Limiting Current Densities of the MFC with the Different Anolyte/Catholyte Flow Rate Ratios

anolyte/catholyte flow rate ratio	peak power density (mW cm^{-2})	limiting current density (mA cm^{-2})
1:1	113.99	414.13
2:1	191.94	591.8
3:1	163.44	471.13

https://doi.org/10.1021/acsomega.2c03840
ACS Omega 2022, 7, 28646−28657

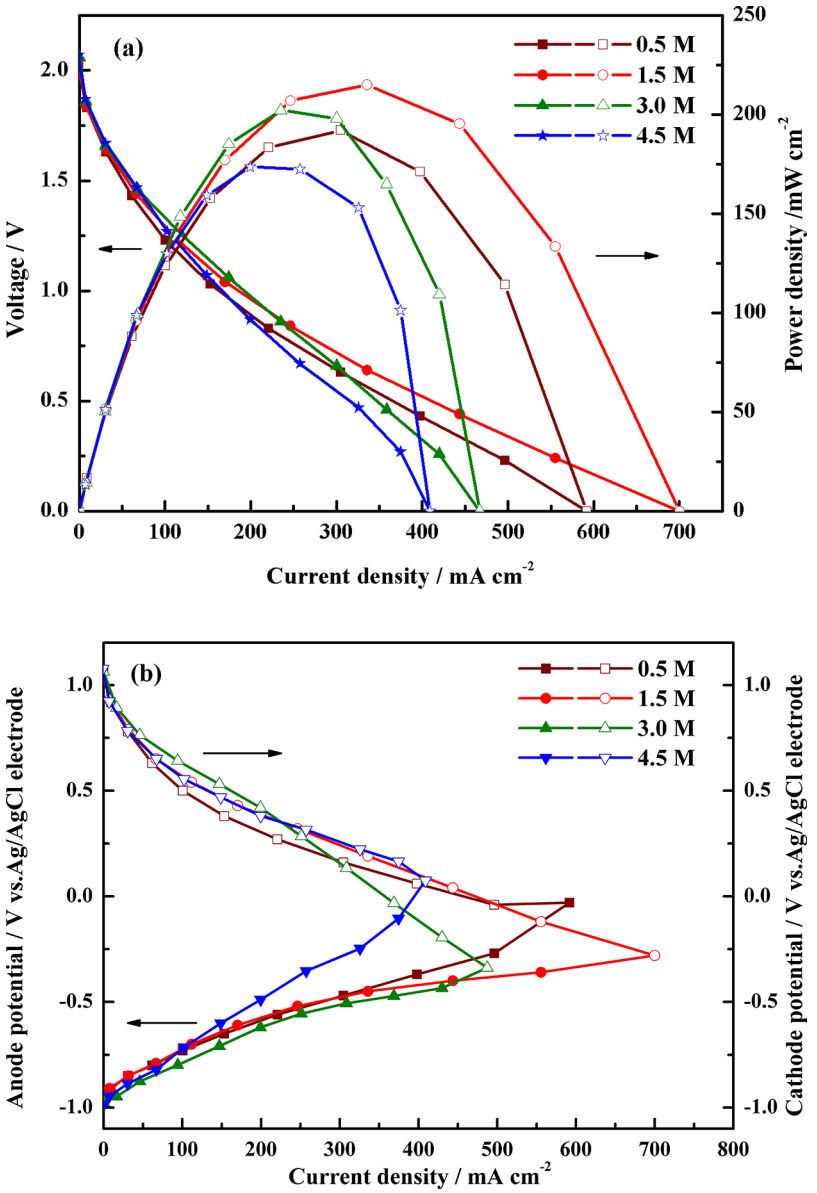

Figure 7. Polarization curves (a) and electrode potentials curves (b) of the $Na_2S_2O_8$-based MFC with the different formate concentrations.

the lower oxidant flow rate, decreasing the cathode potentials. Thus, under the flow ratio of 2:1, the MFC performance was the best.

3.4. Effect of Fuel Concentrations on the Performance of the $Na_2S_2O_8$-Based MFC. Fuel concentration is also a key factor affecting the performance of the MFCs. The effects of the fuel concentrations on the $Na_2S_2O_8$-based MFC are shown in Figure 7. The fuel concentrations arose from 0.5 to 4.5 M. The catholyte was a 2.0 M $Na_2S_2O_8$ + 1.0 M H_2SO_4 solution and the total flow rate was fixed at 300 μL min^{-1} under the anolyte/catholyte flow ratio of 2:1.

With the increase in the fuel concentration from 0.5 to 1.5 M, the cell performance was improved. When the fuel concentration was further increased to 4.5 M, the cell performance substantially decreased. At 1.5 M formate, the performance of the $Na_2S_2O_8$-based MFC was the optimum, with the peak power density of 214.95 mW cm^{-2} and limiting current density of 700.13 mA cm^{-2}. The maximum power density at 1.5 M HCOONa was 1.12, 1.06, and 1.14 times that at 0.5, 3.0, and 4.5 M HCOONa, respectively, and the largest current density at 1.5 M formate was 1.18 times that at 0.5 M, 1.50 times that at 3.0 M, and 1.75 times that at 4.5 M, respectively. The peak power densities and limiting current densities of the MFCs with the different formate concentrations are listed in Table 5.

From the potential curves (Figure 7b) under the different fuel concentrations, the discrepancy in cell performance mainly could be ascribed to the anode electrode potentials, especially

Table 5. Peak Power Densities and Limiting Current Densities of the MFCs with the Different Formate Concentrations

formate concentration	peak power density (mW cm^{-2})	limiting current density (mA cm^{-2})
0.5 M	191.94	591.80
1.5 M	214.95	700.13
3.0 M	190.99	473.75
4.5 M	173.54	408.93

https://doi.org/10.1021/acsomega.2c03840
ACS Omega 2022, 7, 28646−28657

at high current densities. At the high current densities, anodic potentials at 1.5 M formate were more negative than those at 0.5 M formate as the higher fuel concentrations enhanced the anodic oxidant reaction. When the fuel concentrations were larger than 1.5 M, the anodic potentials became more positive under the high current densities and the anode performance declined since the conductivity of the fuel solution decreased.[11]

The CV measurements of formate oxidation reactions on the anode under the different fuel concentrations are shown in Figure 8. From Figure 8, it could be seen that the oxidation currents at 1.5 M formate were larger than those at the other formate concentrations. The CV results also verified the effects of the fuel concentrations on the MFC performance.

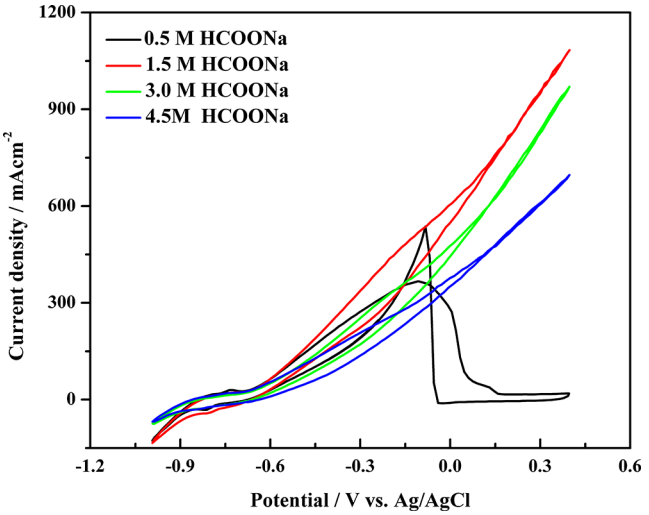

Figure 8. CV curves of formate oxidation reactions on the anode under the different fuel concentrations.

In this paper, we compared the performance of our MFC and others' work, shown in Table 6. It obviously could be seen that the MFC with $Na_2S_2O_8$ as the oxidant shows the highest OCV (~2.0 V), and our $Na_2S_2O_8$-based MFC displayed the highest peak power density and limiting current density. These values also were the largest in the previously reported direct formic acid and formate MFCs.

It was worth noting that the performance of our $Na_2S_2O_8$-based MFC was better than that of the $Na_2S_2O_8$-based MFC by Lan.[14] This was mainly due to the different hydrophilic treatment of the carbon paper electrode. In our work, we activated the carbon paper by the heat treatment at 450 °C for 10 h, while in Lan's work,[14] they treated the carbon paper by the electrochemical activation in a 1 M H_2SO_4 solution. To demonstrate the difference in the electrochemical performances of the electrodes by the different treatment methods, we compared the electrochemical features of the treated electrodes in the formate and persulfate solution, respectively. The results are shown in Figures S1 and S2 in Supporting Materials. From these figures, it could be seen that the carbon paper electrode by the heat treatment showed stronger oxidation in the anolyte or reduction in the catholyte than that by the electrochemical treatment.

Fuel utilization is one of the important parameters that reflects the performance of MFCs. The maximum fuel utilization rate can be calculated according to the formula[2,14] given below

$$\eta = j/(nFC_0Q) \quad (2)$$

Here, η is the maximum fuel utilization, j is the limiting current, n is the number of transferred electrons for the oxidation of formate (n = 2), F is the Faraday constant (96485 C mol^{-1}), C_0 is the initial fuel concentration, and Q is the flow rate of the fuel solution. The curve of η with C_0 is shown in Figure 9. It could be seen that η decreased with the increase of

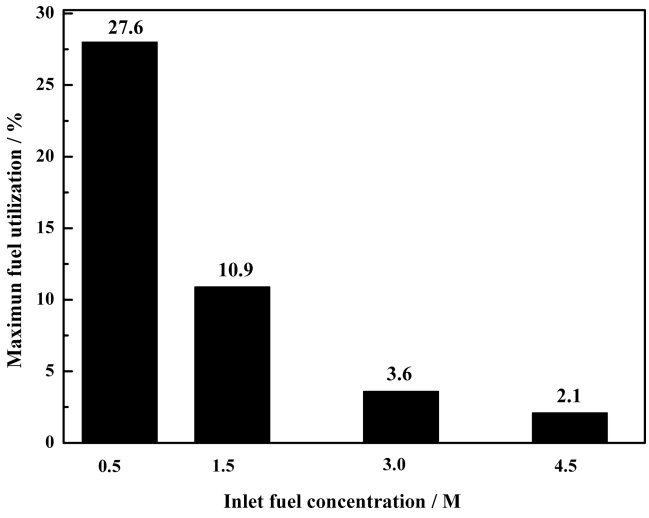

Figure 9. Plot of the maximum fuel utilization with the inlet fuel concentrations under the oxidant solution of 2.0 M $Na_2S_2O_8$ + 1.0 M H_2SO_4, the total flow rate of 300 μL min^{-1}, and the anolyte/catholyte flow rate ratio of 2:1.

Table 6. Comparison of the Performance of the Reported Direct Formic Acid and Formate MFCs

fuel	oxidant/eletrolye	cathode catalyst	open-circuit voltage (V)	peak power density (mW cm^{-2})	limiting current density (mA cm^{-2})	ref
HCOOH	O_2 (g)/H_2SO_4	Pt black	0.9	26	130	11
HCOOH	O_2 (g) /H_2SO_4	Pt black	1.08	22.2	142.2	40
HCOOH	H_2O_2/H_3PO_4	Pt	1.1	30	150	12
HCOOH	$KMnO_4$/H_2SO_4	none	1.35	26	not mentioned	26
HCOOH	Fe^{3+}/HCl	none	0.82	3.9	17.7	28
HCOONa	O_2 (g)/ KOH	Pt black	~0.95	46.6	288.4	41
HCOONa	$NaClO_4$/NaOH	Au	1.42	52	230	25
HCOONa	H_2O_2/H_2SO_4	Pd	1.41	24.75	74.56	42
HCOONa	$Na_2S_2O_8$/H_2SO_4	none	2.0	148	450	14
HCOONa	$FeCl_3$/H_2SO_4	none	1.5	89.27	236.87	this work
HCOONa	$Na_2S_2O_8$/H_2SO_4	none	2.0	214.95	700.13	this work

https://doi.org/10.1021/acsomega.2c03840
ACS Omega 2022, 7, 28646−28657

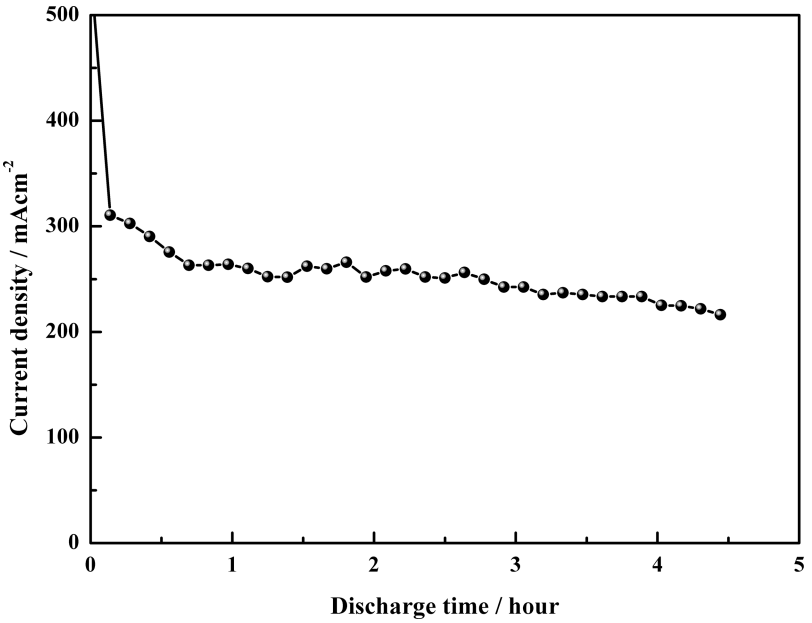

Figure 10. Discharge performance of the $Na_2S_2O_8$-based MFC under the constant cell voltage of 0.64 V.

C_0. This trend was consistent with Zhang.[43] The maximum η of 27.6% was achieved at 0.5 M formate, about 13.8 times as high as that of 2.1% at 4.5 M formate. As the oxidation reaction of formate only occurred on the interface between the electrode and electrolyte, only the fuel near the electrode took part in the reaction and that far from the electrode did not participate and directly flew out of the MFC. Hence, although a higher fuel concentration could enhance its electrochemical kinetics, fuel consumption was inconsistent with the fuel input, leading to a decrease in the fuel utilization. In addition, the maximum fuel utilization rate was the highest at 0.5 M HCOONa, while the performance of the $Na_2S_2O_8$-based MFC was the optimum at 1.5 M HCOONa. This tradeoff between the power density and the maximum fuel utilization needs to be further considered.

3.5. Discharge Performance of the Direct Formate-$Na_2S_2O_8$ MFC. To evaluate the stable discharge performance of the direct formate-$Na_2S_2O_8$ MFC, the cell was discharged under the constant cell voltage of 0.64 V, and then the current densities were recorded, as shown in Figure 10. This voltage (0.64 V) was that corresponding to the peak power density of the optimum MFC performance. The experimental conditions of the best MFC performance were gained for the 1.5 M HCOONa + 2 M NaOH solution and 2.0 M $Na_2S_2O_8$ + 1 M H_2SO_4 solution, at the total flow rate of 300 μL min^{-1}, and the anolyte/catholyte flow rate ratio of 2:1.

At the initial stage of the discharge curve, there existed a higher current density (523.03 mA cm^{-2}), due to the double-layer charging, adsorption of high concentration, and the intimate contact of formate with the active site of the electrode.[44,45] At about 0.5 h, the current densities decreased rapidly from 523.03 to 275.72 mA cm^{-2}, due to the formation of CO_{ads} and the other intermediate species during the formate oxidation reaction.[45,46] The accumulation of the above species reduced the adsorption of OH_{ads} and lowered the active sites, largely decreasing the current densities. During the rest of the discharge time (about 4 h), the MFC kept relatively stable with an average value of 247.48 mA cm^{-2}. The current density dropped slowly to 216.13 mA cm^{-2} at the discharge end due to the reduction of the Pd catalyst activation[43] under the long operation time.

Except for the beginning of discharge from 0.5 h, the relative degradation rate for most (about 4 h) of the discharge time was 5.4%/h, which was larger than that (3.6%/h) in the vapor-feed MFC.[48] The reason for this difference was that the oxidant ($Na_2S_2O_8$) used in our experiment was liquid, while the oxidant (air) used in the vapor-feed MFC[47] was gaseous. The liquid oxidant and fuel could directly contact in the liquid−liquid interface in the main channel of the MFC, increasing the chance of the reactant crossover and the difficulty in keeping the two solutions flow steadily. To decrease the reactant crossover and gain more stable discharge performance, we can adopt the separator[48] or introduce the third solution[49] to separate the anolyte and catholyte in the MFC in further research.

4. CONCLUSIONS

To obtain an MFC with high power output and low cost, we constructed two direct formate MFCs with catalyst-free oxidants $FeCl_3$ and $Na_2S_2O_8$, and then compared the performance of the two MFCs. The experimental results showed that the open-circuit voltage of the direct formate/sodium persulfate microfluidic fuel cell was higher (>2.0 V) and its performance was better. The maximal power density of the $Na_2S_2O_8$-based MFC was 1.17 times that of the $FeCl_3$-based MFC. Then, aimed at the $Na_2S_2O_8$-based MFC, we have studied the oxidant concentrations, flow rates, fuel concentrations on the performance of the direct formate/sodium persulfate MFC. When the $Na_2S_2O_8$ concentration was 2 M, the total flow rate was 300 μL min^{-1}, the anolyte/catholyte flowing rate ratio was 2:1, and fuel concentration was 1.5 M, the $Na_2S_2O_8$-based direct formate MFC achieved the best performance with the peak power density of 214.95 mW cm^{-2} and limiting current density of 700.13 mA cm^{-2}. Also, the discharge curve of the $Na_2S_2O_8$-based MFC showed this MFC could stably discharge in the most of the discharge time. All these results presented $Na_2S_2O_8$ was a suitable oxidant adopted in the MFCs and the $Na_2S_2O_8$-based MFC displayed high

https://doi.org/10.1021/acsomega.2c03840
ACS Omega 2022, 7, 28646−28657

performance, low cost and relatively stable discharge, which assured the feasible application of the $Na_2S_2O_8$-based MFC as a micropower device.

In the further study, we will focus on how to well tradeoff between the fuel utilization and power density. And how to achieve high power density under the high fuel concentrations is our another research topic.

■ ASSOCIATED CONTENT

Supporting Information

The Supporting Information is available free of charge at https://pubs.acs.org/doi/10.1021/acsomega.2c03840.

CV curves (Figure S1) of the electrodes by the two treatment methods in the anolyte and LSV curves (Figure S2) of the electrodes by the two treatments in the catholyte (PDF)

■ AUTHOR INFORMATION

Corresponding Author

Chunmei Liu − *College of Vehicle and Traffic Engineering, Henan University of Science and Technology, Luoyang 471003 Henan Province, China*; orcid.org/0000-0003-0877-1427; Phone: +86 379 64230418; Email: liuchm800226@163.com

Authors

Yanjun Gao − *College of Vehicle and Traffic Engineering, Henan University of Science and Technology, Luoyang 471003 Henan Province, China*

Lei Liu − *China Nonferrous Metals Processing Technology Co., Ltd., Luoyang 471003 Henan Province, China*

Canxing Sun − *College of Vehicle and Traffic Engineering, Henan University of Science and Technology, Luoyang 471003 Henan Province, China*

Pengfei Jiang − *College of Vehicle and Traffic Engineering, Henan University of Science and Technology, Luoyang 471003 Henan Province, China*

Jingjie Liu − *College of Vehicle and Traffic Engineering, Henan University of Science and Technology, Luoyang 471003 Henan Province, China*

Complete contact information is available at: https://pubs.acs.org/10.1021/acsomega.2c03840

Author Contributions

C.L.: Supervision, Writing original draft, Funding acquisition. Y.G.: Investigation, Data curation. L.L.: Design of the MFC. C.S.: Validation. P.J.: Validation. J.L.: Validation.

Notes

The authors declare no competing financial interest.

■ ACKNOWLEDGMENTS

This work is financially supported by the National Natural Science Foundation of China (51506046), Henan young backbone teachers project in 2018 (2018GGJS046), Key scientific research projects of colleges and universities in Henan Province in 2022 (22B470004).

■ REFERENCES

(1) Ferrigno, R.; Stroock, A. D.; Clark, T. D.; Mayer, M.; Whitesides, G. M. Membraneless vanadium redox fuel cell using laminar flow. *J. Am. Chem. Soc.* **2002**, *124*, 12930−12931.

(2) Mousavi Shaegh, S. A.; Nguyen, N.-T.; Chan, S. H. A review on membraneless laminar flow-based fuel cells. *Int. J. Hydrogen Energy* **2011**, *36*, 5675−5694.

(3) Kjeang, E.; Djilali, N.; Sinton, D. Microfluidic fuel cells: A review. *J. Power Sources* **2009**, *186*, 353−369.

(4) Goulet, M. A.; Kjeang, E. Co-laminar flow cells for electrochemical energy conversion. *J. Power Sources* **2014**, *260*, 186−196.

(5) Zhou, Y.; Zhu, X.; Yang, Y.; Ye, D. D.; Chen, R.; Liao, Q. Route towards high-performance microfluidic fuel cells: a review. *Sustainable Energy Fuels* **2021**, *5*, 2840−2859.

(6) Wang, Y. F.; Luo, S. J.; Kwok, H. Y. H.; Pan, W. D.; Zhang, Y. G.; Zhao, X. L.; Leung, D. Y. C. Microfluidic fuel cells with different types of fuels: A prospective review. *Renewable Sustainable Energy Rev.* **2021**, *141*, No. 110806.

(7) Mitrovski, S. M.; Nuzzo, R. G. A passive microfluidic hydrogen-air fuel cell with exceptional stability and high performance. *Lab Chip* **2006**, *6*, 353−361.

(8) Mitrovski, S. M.; Elliott, L. C.; Nuzzo, R. G. Microfluidic devices for energy conversion: planar integration and performance of a passive, fully immersed H_2-O_2 fuel cell. *Langmuir* **2004**, *20*, 6974−6976.

(9) Choban, E. R.; Spendelow, J. S.; Gancs, L.; Wieckowski, A.; Kenis, P. J. A. Membraneless laminar flow-based micro fuel cells operating in alkaline, acidic, and acidic/alkaline media. *Electrochim. Acta* **2005**, *50*, 5390−5398.

(10) Choban, E. R.; Waszczuk, P.; Kenis, P. J. A. Characterization of limiting factors in laminar flow-based membraneless microfuel cells. *Electrochem. Solid-State Lett.* **2005**, *8*, No. A348.

(11) Jayashree, R. S.; Gancs, L.; Choban, E. R.; Primak, A.; Natarajan, D.; Markoski, L. J.; Kenis, P. J. Air-breathing laminar flow-based microfluidic fuel cell. *J. Am. Chem. Soc* **2005**, *127*, 16758−16759.

(12) Kjeang, E.; Brolo, A. G.; Harrington, D. A.; Djilali, N.; Sinton, D. Hydrogen peroxide as an oxidant for microfluidic fuel cells. *J. Electrochem. Soc.* **2007**, *154*, B1220−B1226.

(13) Liu, Z.; Ye, D. D.; Zhu, X.; Wang, S.; Chen, R.; Yang, Y.; Liao, Q. A self-pumping microfluidic fuel cell powered by formate with Pd coated carbon cloth electrodes. *J. Power Sources* **2021**, *490*, 229553−229560.

(14) Lan, Q.; Ye, D. D.; Zhu, X.; Chen, R.; Liao, Q.; Zhang, T.; Zhou, Y. Direct formate/persulfate microfluidic fuel cell with a catalyst-free cathode and high power density. *ACS Sustainable Chem. Eng.* **2021**, *9*, 5623−5630.

(15) Kjeang, E.; Michel, R.; Harrington, D. A.; Djilali, N.; Sinton, D. A microfluidic fuel cell with flow-through porous electrodes. *J. Am. Chem. Soc.* **2008**, *130*, 4000−4006.

(16) Kjeang, E.; Proctor, B. T.; Brolo, A. G.; Harrington, D. A.; Djilali, N.; Sinton, D. High-performance microfluidic vanadium redox fuel cell. *Electrochim. Acta* **2007**, *52*, 4942−4946.

(17) Yan, X. H.; Xu, A.; Zeng, L.; Gao, P.; Zhao, T. S. A Paper-Based Microfluidic fuel cell with hydrogen peroxide as fuel and oxidant. *Energy Technol.* **2018**, *6*, 140−143.

(18) Yang, Y.; Xue, Y. S.; Zhang, H.; Chang, H. L. Flexible H_2O_2 microfluidic fuel cell using graphene/Prussian blue catalyst for high performance. *Chem. Eng. J.* **2019**, *369*, 813−817.

(19) Kundu, A.; Jang, J. H.; Gil, J. H.; Jung, C. R.; Lee, H. R.; Kim, S. -H.; Ku, B.; Oh, Y. S. Micro-fuel cells-current development and applications. *J. Power Sources* **2007**, *170*, 67−78.

(20) Morse, J. D. Micro-fuel cell power sources. *Int. J. Energy Res.* **2007**, *31*, 576−602.

(21) Zhu, Y.; Khan, Z.; Masel, R. I. The behavior of palladium catalysts in direct formic acid fuel cells. *J. Power Sources* **2005**, *139*, 15−20.

(22) Bianchini, C.; Shen, P. K. Palladium-based electrocatalysts for alcohol oxidation in half cells and in direct alcohol fuel cells. *Chem. Rev.* **2009**, *109*, 4183−4206.

(23) Marchionni, A.; Bevilacqua, M.; Bianchini, C.; Chen, Y. X.; Filippi, J.; Fornasiero, P.; Lavacchi, A.; Miller, H.; Wang, L.; Vizza, F.

Electrooxidation of ethylene glycol and glycerol on Pd-(Ni-Zn)/C anodes in direct alcohol fuel cells. *ChemSusChem* **2013**, *6*, 518−528.
(24) Pramanik, H.; Rathoure, A. K. Electrooxidation study of $NaBH_4$ in a membraneless microfluidic fuel cell with air breathing cathode for portable power application. *Int. J. Hydrogen Energy* **2017**, *42*, 5340−5350.
(25) Kjeang, E.; Michel, R.; Harrington, D. A.; Sinton, D.; Djilali, N. An alkaline microfluidic fuel cell based on formate and hypochlorite bleach. *Electrochim. Acta* **2008**, *54*, 698−705.
(26) López-Montesinos, P.; Yossakda, N.; Schmidt, A.; Brushett, F. R.; Pelton, W. E.; Kenis, P. J. A. Design, fabrication, and characterization of a planar, silicon-based, monolithically integrated micro laminar flow fuel cell with a bridge-shaped microchannel cross-section. *J. Power Sources* **2011**, *196*, 4638−4645.
(27) Zeng, L.; Sun, J.; Zhao, T. S.; Ren, Y. X.; Wei, L. Balancing the specific surface area and mass diffusion property of electrospun carbon fibers to enhance the cell performance of vanadium redox flow battery. *Int. J. Hydrogen Energy* **2020**, *45*, 12565−12576.
(28) Liu, C. M.; Liu, L.; Wang, X. T.; Xu, B.; Lan, W. J. Enhancing the performance of microfluidic fuel cells by modifying the carbon-fiber paper cathode by air annealing and acid oxidation. *Ind. Eng. Chem. Res.* **2018**, *57*, 13557−13565.
(29) Liu, C. M.; Liao, Q.; Zhu, X.; Yang, Y. Investigating the composition of iron salts on the performance of microfluidic fuel cells. *Ind. Eng. Chem. Res.* **2018**, *57*, 1756−1762.
(30) Choban, E. Microfluidic fuel cell based on laminar flow. *J. Power Sources* **2004**, *128*, 54−60.
(31) Chandra, S.; Lal, S.; Janardhanan, V. M.; Sahu, K. C.; Deepa, M. Ethanol based fuel cell on paper support. *J. Power Sources* **2018**, *396*, 725−733.
(32) Liu, C. M.; Liu, H. H.; Liu, L. Potassium permanganate as an oxidant for a microfluidic direct formate fuel cell. *Int. J. Electrochem. Sci.* **2019**, *14*, 4557−4570.
(33) Braff, W. A.; Bazant, M. Z.; Buie, C. R. Membrane-less hydrogen bromine flow battery. *Nat. Commun.* **2013**, *4*, No. 2346.
(34) Ike, I. A.; Linden, K. G.; Orbell, J. D.; Duke, M. Critical review of the science and sustainability of persulphate advanced oxidation processes. *Chem. Eng. J.* **2018**, *338*, 651−669.
(35) Chen, X.; Oh, W. D.; Lim, T. T. Graphene- and CNTs-based carbocatalysts in persulfates activation: Material design and catalytic mechanisms. *Chem. Eng. J.* **2018**, *354*, 941−976.
(36) Li, J.; Fu, Q.; Liao, Q.; Zhu, X.; Ye, D. D.; Tian, X. Persulfate: A self-activated cathodic electron acceptor for microbial fuel cells. *J. Power Sources* **2009**, *194*, 269−274.
(37) Li, N.; Tang, S. F.; Rao, Y. D.; Qi, J. B.; Wang, P. K.; Jiang, Y.; Huang, H. M.; Gu, J. M.; Yuan, D. L. Improved dye removal and simultaneous electricity production in a photocatalytic fuel cell coupling with persulfate activation. *Electrochim. Acta* **2018**, *270*, 330−338.
(38) Liang, C.; Wang, Z. S.; Bruell, C. J. Influence of pH on persulfate oxidation of TCE at ambient temperatures. *Chemosphere* **2007**, *66*, 106−113.
(39) Thimmappa, R.; Devendrachari, M. C.; Kottaichamy, A. R.; Aralekallu, S.; Gautam, M.; Shafi, S. P.; Bhat, Z. M.; Thotiyl, M. O. 2.6 V aqueous battery with a freely diffusing electron acceptor. *J. Phys. Chem. C* **2017**, *121*, 3707−3713.
(40) Zhang, B.; Ye, D. D.; Li, J.; Zhu, X.; Liao, Q. Air-breathing microfluidic fuel cells with a cylinder anode operating in acidic and alkaline media. *Electrochim. Acta* **2015**, *177*, 264−269.
(41) Zhang, T.; Zhu, X.; Ye, D. D.; Chen, R.; Zhou, Y.; Liao, Q. Cyclic voltammetry electrodeposition of well-dispersed Pd nanoparticles on carbon paper as a flow-through anode for microfluidic direct formate fuel cells. *Nanoscale* **2020**, *12*, 20270−20278.
(42) Sankar, S.; Anilkumar, G. M.; Tamaki, T.; Yamaguchi, T. Cobalt-modified palladium bimetallic catalyst: a multifunctional electrocatalyst with enhanced efficiency and stability toward the oxidation of ethanol and formate in alkaline medium. *ACS Appl. Energy Mater.* **2018**, *1*, 4140−4149.
(43) Zhang, H.; Xuan, J.; Xu, H.; Leung, M. K. H.; Leung, D. Y. C.; Zhang, L.; Wang, H. Z.; Wang, L. Enabling high-concentrated fuel operation of fuel cells with microfluidic principles: A feasibility study. *Appl. Energy* **2013**, *112*, 1131−1137.
(44) Wang, Z. B.; Yin, G. P.; Zhang, J.; Sun, Y. C.; Shi, P. F. Investigation of ethanol electrooxidation on a Pt-Ru-Ni/C catalyst for a direct ethanol fuel cell. *J. Power Sources* **2006**, *160*, 37−43.
(45) Raj kumar, T.; Gnana kumar, G.; Manthiram, A. Biomass-derived 3D carbon aerogel with carbon shell-confined binary metallic nanoparticles in CNTs as an efficient electrocatalyst for microfluidic direct ethylene glycol fuel cells. *Adv. Energy Mater.* **2019**, *9*, No. 1803238.
(46) Xu, H.; Yan, B.; Wang, J.; Zhang, K.; Li, S.; Xiong, Z.; Wang, C.; Shiraishi, Y.; Du, Y.; Yang, P. Self-supported porous 2D AuCu triangular nanoprisms as model electrocatalysts for ethylene glycol and glycerol oxidation. *J. Mater. Chem. A* **2017**, *5*, 15932−15939.
(47) Wang, Y. F.; Leung, D. Y. C.; Hu, S. Durability and stability of vapor-feed microfluidic fuel cells, a preliminary study. *Energy Procedia* **2017**, *142*, 1340−1345.
(48) Wang, S. L.; Ye, D. D.; Liu, Z. F.; Chen, R.; Zhu, X.; Zhang, B.; Wu, R.; Liao, Q. A direct formate microflfluidic fuel cell with cotton thread-based electrodes. *Int. J. Hydrogen Energy* **2020**, *45*, 27665−27674.
(49) Zhu, X.; Zhang, T.; Yu, C. H.; Yang, Y.; Ye, D. D.; Chen, R.; Liao, Q. Filter paper membrane based microflfluidic fuel cells: Toward next-generation miniaturized and low cost power supply. *Int. J. Hydrogen Energy* **2022**, *47*, 15065−15073.

https://doi.org/10.1021/acsomega.2c03840
ACS Omega 2022, 7, 28646−28657